JOURNAL OF PROPULSION AND POWER
Vol. 17, No. 1, January–February 2001

Fundamental Studies of Cavity-Based Flameholder Concepts for Supersonic Combustors

M. R. Gruber*
U.S. Air Force Research Laboratory, Wright–Patterson Air Force Base, Ohio 45433
R. A. Baurle† and T. Mathur†
Taitech, Inc., Beavercreek, Ohio 45430
and
K.-Y. Hsu‡
Innovative Scientific Solutions, Inc., Dayton, Ohio 45440

Experimental and computational investigations of the flowfield associated with several cavity-based flameholders in a nonreacting supersonic flow are described. All cavity flows were of the open type, that is, length-to-depth ratio $L/D < 10$. Two values of L/D were studied with several offset ratios (OR) and aft ramp angles θ. Results indicate that the aft ramp angle plays an important role in determining the character of the shear layer that spans the cavity. For a rectangular cavity with OR = 1 and $\theta = 90$ deg, a compression wave forms as the flow separates from the cavity's upstream corner. A strong recompression occurs at the aft wall, and the flow is visibly unsteady. The pressure on the cavity fore wall decreases steadily and the recompression process occurs more gradually with decreasing aft ramp angle. Higher drag coefficients and shorter residence times are found in cavities with shallower ramp angles.

Nomenclature

D_d	=	downstream step height
D_u	=	upstream step height
k	=	turbulent kinetic energy
L/D, L/D_u	=	cavity length-to-depth ratio
m	=	mass
OR	=	offset ratio, D_u/D_d
P	=	static pressure
P_∞	=	freestream static pressure
t	=	time
x	=	streamwise position
y^+	=	wall coordinate
θ	=	aft ramp angle
κ	=	MUSCL parameter
τ	=	cavity residence time
ω	=	turbulent frequency

Introduction

FUEL injection, ignition, and flameholding present fundamental challenges to the design of a hydrocarbon-fueled supersonic combustion ramjet (scramjet) engine. To achieve efficient combustion within a manageable length, a successful fuel injection scheme must provide rapid mixing between the fuel and airstreams. However, the introduction of fuel into the combustor must be carried out in such a way that the airstream suffers acceptable total pressure losses. Another challenge associated with combustion in scramjets is to provide a stable flameholding system. This implies that the fuel–air mixture within the flameholder is appropriate and controllable over a wide range of operating conditions, that is, velocity, pressure, and temperature.

Received 20 May 1999; presented as Paper 99-2248 at the AIAA 35th Joint Propulsion Conference, Los Angeles, CA, 20–24 June 1999; revision received 1 February 2000; accepted for publication 8 February 2000.

*Aerospace Engineer, Propulsion Directorate, 1790 Loop Road North. Senior Member AIAA.
†Research Scientist, 1430 Oak Court, Suite 301. Member AIAA.
‡Senior Engineer, 2786 Indian Ripple Road. Member AIAA.

To date, these problems have not been adequately resolved. Flush-wall and parallel injection concepts have been investigated, each with its merits and drawbacks. In addition, many injection schemes that impose significant pressure losses to achieve flameholding have been explored. These devices add high levels of complexity to the system, for example, active cooling systems for preservation of sharp leading edges, etc. A clear need exists for the development of a system that effectively integrates fuel injection and flameholding for supersonic combustion with minimal system complexity and performance detriment.

Background

Several factors are important in the development of a suitable flameholder for a dual-mode scramjet combustor, including static pressure in the flameholder, entrainment rate, residence time, and drag. Higher static pressure is expected to improve the performance of a typical flameholder. In the dual-mode scramjet, a relatively strong pressure rise will be experienced inside the combustor. The energy addition from combustion of the hydrocarbon fuel causes the approaching supersonic flow to decelerate through a series of shock waves, thereby increasing its static pressure. In previous work using ethylene in a model scramjet operating at conditions that simulate Mach 4–5 flight conditions, the peak pressure has been observed to occur at a location inside the flameholding device.[1,2] Thus, at low flight Mach numbers, the benefits of high static pressure near the flameholder should be achievable. Also, in the dual-mode scramjet, it is desirable to minimize the drag generated by the flameholding system because thrust margins are generally small. Winterfeld[3] studied several flameholder geometries and showed that flameholders characterized by greater flow deflections produced faster exchange rates. He also found that for a fixed flameholder shape, increasing blockage, that is, drag, resulted in a decrease in residence time and an increase in exchange rate. These observations illustrate the compromise that must be accepted in the development of flameholders for scramjets.

Three recent publications have presented comprehensive literature surveys on cavity flows and their relevance for flameholders in supersonic combustion engines.[4–6] Experimental and analytical research to date has predominantly examined the role of cavities in external flows,[7–27] although there have been studies examining

the flameholding characteristics in low-speed[28,29] and high-speed flows.[4–6,30–36]

Cavity flows generally fall into one of two categories: open or closed. These two flowfields are illustrated schematically in Fig. 1. In open cavity flows (Fig. 1a), the shear layer formed at the separation corner spans the entire cavity length and reattaches somewhere along the cavity back face. These cavities generally have low values of drag, but also relatively small levels of entrainment from the main flow. Closed cavity flows (Fig. 1b) occur when the shear layer is unable to span the entire length of the cavity and reattaches on the cavity floor. Closed cavities are characterized by larger drag coefficients compared with open cavities. Therefore, due to their lower drag penalty, open cavities are more desirable in a scramjet combustor. The length-to-depth ratio that separates open and closed behavior is typically between 10 and 12 (Ref. 37). In addition to this operational transition, another interesting feature of cavity flows involves the mode by which acoustic waves propagate inside the cavity. Zhang and Edwards[24] have found that for small values of L/D, a cavity immersed in a supersonic stream is dominated by the transverse mode, where acoustic waves propagate perpendicular to the crossflow. As L/D increases, the oscillation mode changes to longitudinal, where the waves travel along the length of the cavity. The transition between the transverse and longitudinal modes results in a sudden increase in the cavity's form drag coefficient. After the longitudinal mode is established, the form drag coefficient decreases slightly with increasing L/D before increasing dramatically due to the effects of stronger shear-layer recompression on the aft face.

Hsu et al.[29] injected fuel and air into an axisymmetric cavity to achieve low-speed flame stabilization. Stable flames resulted for cavity lengths between 0.45 and 0.65 aft wall diameters. Longer cavities produced unstable flames, whereas shorter cavities lacked enough volume for flameholding. With direct injection of fuel and air, stable combustion was obtained at a cavity aspect ratio that corresponded to minimum drag and minimum entrainment. Similar results were obtained from time-dependent computational fluid dynamics (CFD) calculations, that is, a limited L/D range for achieving a stable flame zone.[28]

Yu et al.[31] studied several cavity configurations in an unheated Mach 2 flow. The influence of cavity geometry on the combustion of a fuel jet injected upstream of the cavity was studied. Initial results suggested that small aspect ratio cavities provide better flameholding than longer cavities with inclined aft ramp angles. Similar work has been in progress at the U.S. Air Force Research Laboratory (AFRL) for some time.[1,2,38] Room temperature gaseous and liquid fuels are injected upstream of a cavity in a supersonic combustor operating at conditions that simulate flight Mach numbers between 4 and 6 and flight dynamic pressures between 23.9 and 95.8 kPa (Ref. 39). Results show good flameholding and rapid flame spreading.[1,2,38]

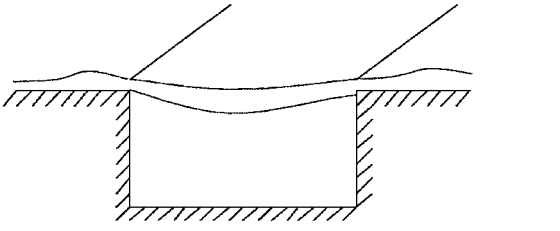

a) Open cavity flow ($L/D < 10$)

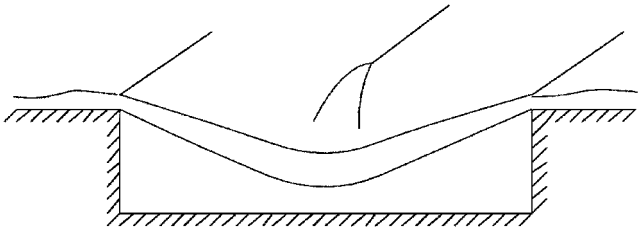

b) Closed cavity flow ($L/D > 10$)

Fig. 1 Character of cavity flows.

Objectives

This investigation is aimed at improving the fundamental understanding of cavity-based flameholders in supersonic flows. The baseline concept uses a wall cavity to provide the stabilization zone. This cavity is described by several parameters including its L/D, aft ramp angle θ, and offset ratio (OR). Simple models of the proposed system are experimentally and numerically studied at one freestream Mach number to identify the important issues in the design of such a device. Included in the initial work are measurements of the wall static pressure distributions throughout the cavity. These measurements are compared directly with CFD results. Conventional flow visualizations are also presented.

Experimental Facility and Diagnostics

Experiments were conducted in the supersonic flow facility located at the AFRL, Propulsion Directorate.[40] A brief facility description is followed by details of the cavity models and the measurement techniques used in this work.

Flow Facility

The flow facility used for these experiments was designed to allow studies of the basic fluid dynamic mechanisms that govern fuel–air mixing in supersonic combustors using conventional and state-of-the-art nonintrusive diagnostic techniques. Figure 2 presents a schematic of the facility. A continuous source of clean compressed air is available to provide stagnation conditions up to 922 K and 5.27 MPa and a total flow rate of about 15.4 kg/s. For these experiments, the planar two-dimensional converging–diverging nozzle section was configured with a pair of Mach 3 half nozzles. The constant-area test section (131 × 152 mm) with fused silica windows mounted in the side walls and the top wall for optical access.

Cavity Flameholder Models

Table 1 presents the geometric features of the cavities studied. All models have the same depth, $D_u = 8.9$ mm, and the length L is

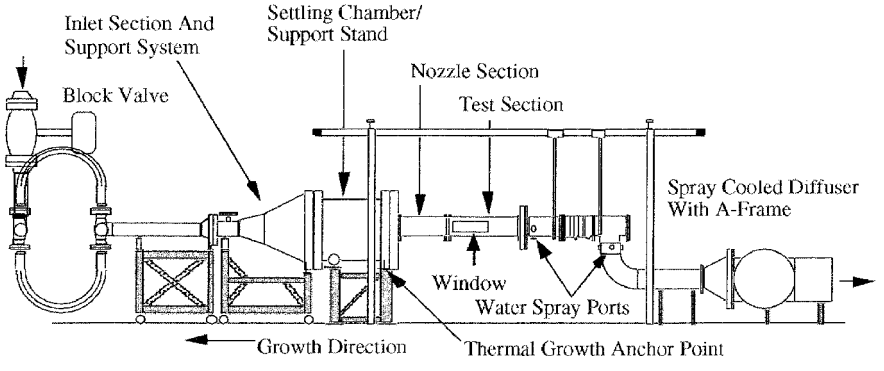

Fig. 2 Facility schematic.

Table 1 Cavity geometry specifications

Name	L/D_u	OR $= D_u/D_d$	Ramp angle θ, deg
LD3-O1-90	3	1	90
LD3-O1-30	3	1	30
LD3-O1-16	3	1	16
LD3-O2-90	3	2	90
LD3-O2-16	3	2	16
LD5-O1-90	5	1	90
LD5-O1-16	5	1	16

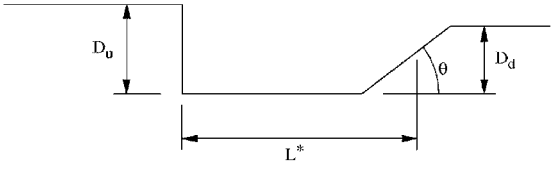

This length is defined as the length of a rectangular cavity or the distance from the leading edge to 0.5(D_d/tan(θ)).

Fig. 3 Cavity geometry schematic.

defined in Fig. 3. The flow direction is from left to right. Instrumentation includes several wall static pressure taps on the fore, bottom, and aft walls. Taps were placed along the spanwise centerline of the model as well as across the span of the cavity at various axial locations. The off-centerline taps provide an indication of the spanwise symmetry of the flow inside the cavity.

Measurement Techniques

Two primary diagnostics were used in this investigation: schlieren and shadowgraph flow visualizations and wall static pressure measurements. A xenon nanolamp (pulse duration ~10 ns) effectively freezes the flowfield, and a PixelVision unintensified charge-coupled device camera records the spatially integrated images. The camera is controlled using a Pentium-based personal computer and the images are stored on disk for further analysis. The schlieren system has a knife edge oriented horizontally so that changes in density in the transverse direction are emphasized. Pressure measurements are obtained from several locations throughout the test section including the fore, bottom, and aft faces of the cavity and the wall opposite the cavity. These measurements are made using traditional pressure taps (0.79-mm diameter) to sense the mean wall static pressure. The taps are connected to a multichannel Pressure Systems Inc. pressure scanning system. The transducers in this system have quoted measurement uncertainties of less than 0.05% of full scale. Data are recorded using a computer-controlled data acquisition system.

Computational Resources

Computational results were obtained using the VULCAN Navier–Stokes code. The code solves the Reynolds-averaged conservation equations appropriate for calorically or thermally perfect gases with a cell-centered finite volume scheme. The equation set can be integrated in a fully elliptic or space-marched manner. The inviscid fluxes can be evaluated with central differences, Roe's flux difference method, or a low-diffusion flux vector split scheme. A variety of one-equation and two-equation turbulence models can be chosen to describe the turbulent velocity field, and assumed probability density function options exist for modeling turbulence–chemistry interactions. Chemically reacting flows can be modeled with global, reduced, or full finite rate kinetics. The code also contains full multigrid capabilities, allowing rapid convergence for steady-state problems. Further descriptions of the code can be found elsewhere.[41]

All calculations were performed using the LDFSS of Edwards.[42] The MUSCL parameter κ was chosen as one-third to minimize truncation error, and the Van Leer flux limiter was used to ensure total variation diminishing. The steady-state solution was advanced in time using a diagonalized approximate factorization scheme; all solutions were advanced with a Courant–Friedrichs–Lewy (CFL) number of 3.5. All simulations assumed that the cavity had infinite span and were, thus, solved using the two-dimensional conservation equations. To match the experimental conditions, the flows were solved without chemical reactions.

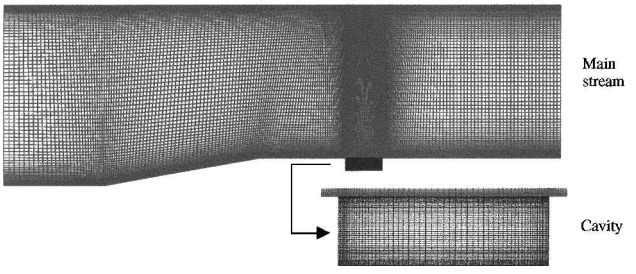

Fig. 4 Sample computational grid.

The turbulence model used for this work was the Wilcox k–ω model.[43] To relax the grid requirements near solid surfaces, the wall matching procedure developed by Wilcox[44] was used. To account for the reduced mixing levels associated with high convective Mach numbers, the compressibility correction of Wilcox[43] was employed. This compressibility correction was chosen over the others (e.g., Zeman[45] and Sarkar et al.[46]) because it does not adversely affect the wall-bounded portions of the flow. A turbulent Prandtl number of 0.89 was used for all simulations.

CFD data were generated for all cavity geometries with OR = 1. Computations were initiated at the facility nozzle plenum and extended to a minimum of ten cavity depths downstream of the cavity trailing edge. When applicable, the parabolized Navier–Stokes equations were utilized to reduce computational costs. The thin-layer Navier–Stokes equations were initially employed in the cavity near field. This reduced equation set was insufficient for describing the complex recirculating flow within the cavity, requiring the use of the full Navier–Stokes equation set. The nozzle inflow conditions were defined by specifying total pressure and temperature and extrapolating velocity from the interior. A zero-gradient assumption was imposed at the supersonic outflow plane downstream of the cavity. All surfaces were assumed adiabatic; calculations neglected spanwise variations.

A typical grid used for the cavity near-field calculations is shown in Fig. 4. The grid zone dimensions for the LD3 geometries were 245×101 in the mainstream and 61×53 within the cavity. The LD5 geometries used grid sizes of 285×101 and 101×53 for the mainstream and cavity, respectively. The grid was refined near all solid surfaces to maintain acceptable limits (y^+ value of cell centers adjacent to solid surfaces less than 50) for wall function formulations. The grids employed for the calculations were found to be sufficient to essentially eliminate grid-related dependencies. All steady-state solutions were advanced in time until the L2 norm of the residual was reduced by at least four orders of magnitude from its initial value. A global mass continuity check revealed the largest relative error to be less than 0.05%. Flowfield variables of interest were also monitored to further ensure that the flow solution had indeed reached steady-state. Typically, this level of convergence required 7500 flow solver iterations (approximately 30 min turnaround time on a Cray T90) using a CFL stability constraint of 3.5.

Results and Discussion

Experiments were conducted with a Mach 3 facility nozzle operated at a stagnation pressure of 690 kPa and a stagnation temperature of 300 K for all of the cavity model experiments and computations discussed in the following sections.

Experimental Visualizations

Figure 5 shows shadowgraph and schlieren photographs of the flowfield in and around each of the seven cavity geometries studied in this investigation. The main flow direction in all photographs is from left to right. The region above the cavity models is free from disturbances that would produce confounding effects in the vicinity of the cavity.

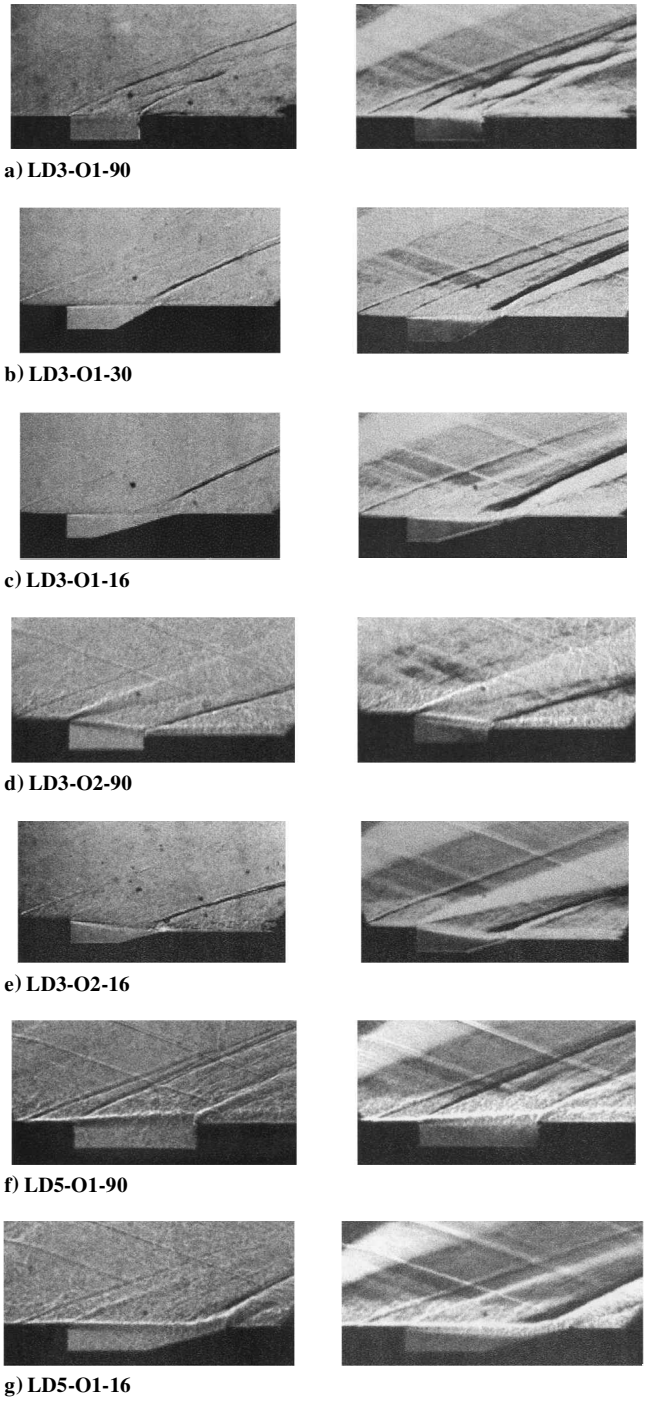

a) LD3-O1-90

b) LD3-O1-30

c) LD3-O1-16

d) LD3-O2-90

e) LD3-O2-16

f) LD5-O1-90

g) LD5-O1-16

Fig. 5 Shadowgraph (left) and schlieren (right) photographs of cavity flowfields.

The visualizations obtained from model LD3-O1-90 (see Table 1) are presented in Fig. 5a. From these photographs, it appears that the approaching boundary-layer thickness is roughly of the same order as the cavity depth. The wave formed at the separation point on the cavity upstream face appears compressive in nature. An expansion wave would appear lighter than the main flow in a schlieren photograph due to the acceleration of the flow and corresponding decrease in density. However, in Fig. 5a, this wave appears darker, indicating a compression wave. The recompression wave at the aft corner of the cavity is also visible. Another interesting feature in these photographs is the curved nature of the waves generated by the cavity, suggesting cavity oscillations. Wave patterns of this type have been recently observed in time-accurate computations.[27] The waves were generated by the oscillatory vortex structure within the cavity.

The effects of decreasing the aft ramp angle to 30 deg for a fixed L/D can be seen in Fig. 5b. The wave emanating from the separation corner remains compressive in nature. Reattachment appears to occur inside the cavity along the aft ramp and the recompression wave is stronger than that shown in Fig. 5a. No oscillatory waves are present, indicating the relative steadiness of the flowfield around this cavity.

Results from model LD3-O1-16 appear in Fig. 5c. Again, no oscillatory waves are present. For this geometry, an expansion wave (as indicated in the schlieren photograph by its light color) is observed at the separation corner. The shear layer extends toward the cavity floor, and the reattachment point is on the face of the aft ramp. The recompression wave appears stronger in this case compared with LD3-O1-90, and the flowfield appears steadier.

Figure 5d shows the shadowgraph and schlieren photographs from the LD3-O2-90 geometry. The most obvious feature in these photographs is the strong expansion fan generated at the separation corner. This is expected because of the downward displacement of the aft wall relative to the forward wall. The shear layer immediately becomes angled with respect to the main flow direction and experiences recompression near the aft corner of the cavity. The flow over this cavity appears steady in comparison with LD3-O1-90. This suggests that increasing the offset ratio influences the behavior of the vortex structure within the cavity, leading to oscillatory behavior in rectangular cavities with unity offset ratio.

When the aft ramp is inclined at 16 deg, the flowfield associated with the OR = 2 cavity becomes similar to that of LD3-O1-16 with the exception of a much stronger expansion fan at the separation corner. Figure 5e shows the representative shadowgraph and schlieren photographs for this geometry. The recompression wave again appears stronger in the case with the 16-deg aft ramp compared with the 90-deg aft ramp (see Figs. 5d and 5e). Also, the flow again appears steady in that no oscillatory waves are evident.

With $L/D = 5$ in a rectangular cavity, the shear layer spanning the cavity is slightly inclined with respect to the crossflow, and a compression wave occurs at the separation corner (see Fig. 5f). Some cavity oscillations are evident.

Figure 5g shows the flow structure of model LD5-O1-16. Oscillatory waves are again absent, indicating a relatively steady flowfield around the cavity. The wave at the separation corner is an expansion wave (as indicated in the schlieren photograph by its light color) of similar strength to the one formed in LD3-O1-16. The shear layer has a slight declination and the recompression point is again on the angled aft ramp. The recompression wave appears stronger in this case when compared with LD5- O1-90.

Computational Visualizations

Pressure contours and cavity stream traces are shown in Fig. 6 for each configuration simulated. The experimental data suggested that the rectangular cavity geometries were characterized by some level of unsteadiness. This is common for cavities of the open type. The calculations, however, did not show any signs of large-scale unsteadiness. This phenomenon is not uncommon when standard eddy-viscosity-based turbulence models are employed for flows of this type.[4,28] Although steady-state flowfields were predicted for the rectangular geometries, the cavity flow structure is markedly different from the shallow aft wall angle geometries. In particular, the rectangular cavity with $L/D = 3$ showed two large counter-rotating vortices, whereas the cavities with angled walls consist of a primary vortex and a smaller secondary vortex near the front wall/bottom wall joint. The larger L/D cavities showed similar trends, although the secondary vortex in LD5-O1-90 was much smaller than in LD3-O1-90.

Wall Pressure Data

Figure 7 shows the distributions of normalized wall static pressure P/P_∞ for all cavities. Measurements are shown as open circles; CFD results appear as solid lines. In Figs. 7a–7g, the wall static pressures are normalized by the freestream static pressure, and the results are plotted as a function of the effective distance (measured from the cavity upstream separation corner along the cavity wall).

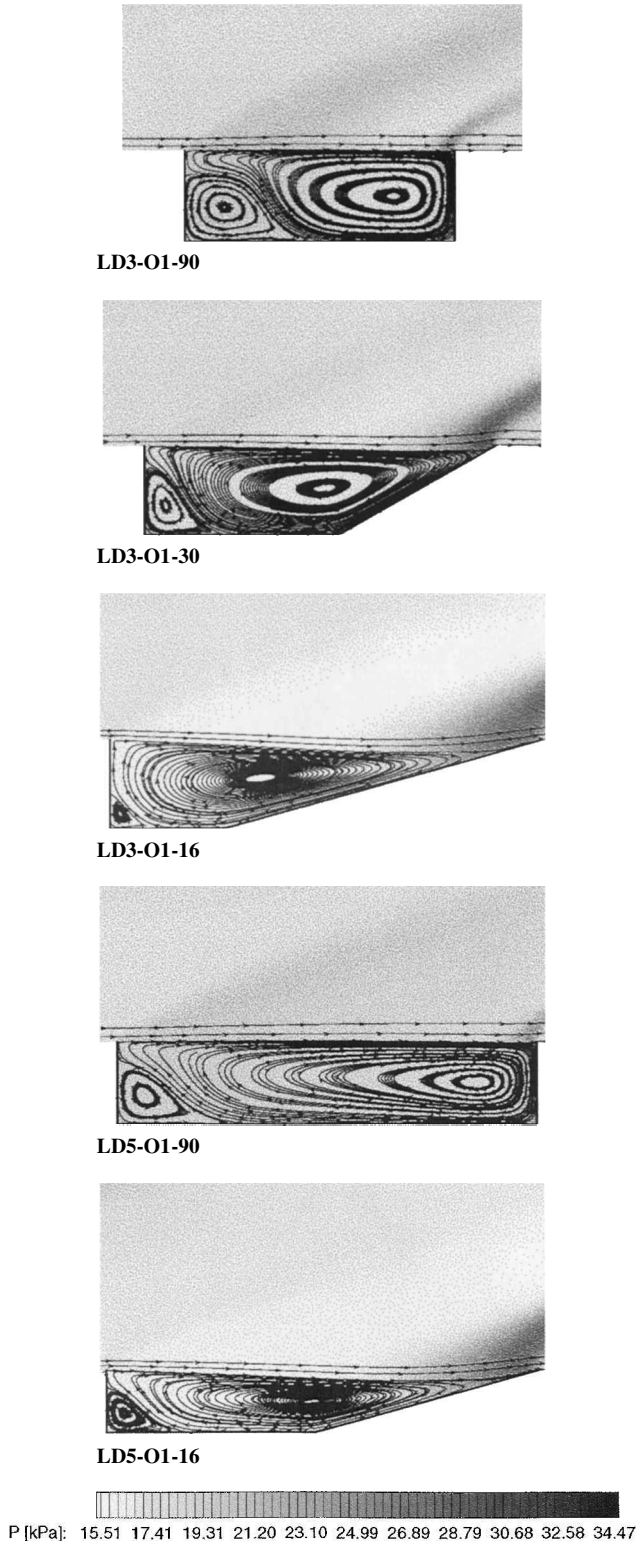

Fig. 6 Computed stream traces and pressure contours.

The plots are divided into fore, bottom, and aft faces using dashed vertical lines. At various locations, several pressure taps were placed at spanwise positions, up to one step height offaxis, to assess the spanwise symmetry of the flow over that region.

The results from LD3-O1-90 appear in Fig. 7a. As noted in Fig. 5a, a compression wave forms at the separation corner resulting in increased pressures (relative to freestream static pressure) in the cavity. Pressure decreases along the cavity bottom wall. The shear layer experiences recompression at the aft wall, leading to higher pressures on the aft face. The CFD result reveals the insufficient spatial resolution of the pressure taps near the cavity aft face. The corner near the cavity floor (effective distance of 1.4 in.) shows this most clearly. The flow in this vicinity mimics an idealized stagnation point flow, resulting in a local pressure peak at the aft wall corner and an increase in cavity form drag.

As the aft angle is decreased to 30 deg (see Fig. 7b), the wave emanating from the separation corner remains compressive (as noted in the visualizations). The behavior within the cavity appears similar to that shown in Fig. 7a, although at a slightly reduced pressure. Finally, the recompression occurs quickly as the shear layer reattaches onto the ramp. Again, the calculation predicts the same reattachment location as observed in the measurements. The pressure data from the taps placed off the cavity centerline collapse well. This suggests that, at least on the cavity centerline, a two-dimensional solution is appropriate. The decrease in ramp angle is accompanied by a weaker pressure rise at the bottom/aft wall corner.

The data presented in Fig. 7c are from LD3-O1-16. In this geometry, the pressure on the forward face of the cavity is lower than that shown in Fig. 7a. This agrees with the visualizations that showed an expansion wave forming at the separation corner. The pressure along the cavity floor is essentially constant at the same level as that of the upstream face. Recompression occurs on the 16-deg ramp leading to locally high pressure levels. Again, numerical results agree closely with measurements, and spanwise symmetry is evident in the experimental data suggesting a high degree of two-dimensionality.

Figures 7d and 7e present the pressure distributions from the cavities with OR = 2. The expansion wave emanating from the separation corner is much stronger than observed with OR = 1. The pressure on the lower wall of the cavity appears to drop slightly as the flow approaches the aft wall, where recompression occurs. Figure 7e shows the effects of decreasing the ramp angle from 90 to 16 deg. The effects are largely confined to the aft wall recompression region. The expansion from the separation corner appears uninfluenced by the reduced ramp angle. Two dimensionality is again suggested from the collapse of the off-centerline pressure data. The low pressure level on the fore wall suggests a relatively large form drag associated with OR = 2 cavity geometries.

Figure 7f shows the results of increasing the L/D to 5 in a rectangular geometry with OR = 1. The compression wave emanating from the separation corner is stronger in LD5-O1-90 as suggested by the higher pressure level on the cavity fore wall. The bottom wall appears to be at a relatively constant pressure until the aft wall, where the vortex structure results in a pressure rise. Finally, recompression causes a higher pressure on the aft wall in this case than in Fig. 7a.

The pressure distributions from LD5-O1-16 appear in Fig. 7g. The expansion wave at the separation corner is similar in strength to the one generated by LD3-O1-16, as inferred from the pressure level on the upstream face of the cavity. The pressure distribution along the cavity bottom wall is relatively constant and recompression appears slightly stronger than in LD3-O1-16. Thus, for a fixed cavity depth, offset ratio, and aft wall ramp angle, the increased length appears to increase the pressure in the recompression region, whereas no influence is observed on the upstream face of the cavity. Therefore, the form drag created by LD5-O1-16 is higher than that of LD3-O1-16. However, because the shear layer length has increased, the entrainment of freestream fluid into the longer cavity is expected to increase.

Overall, the calculations reproduced all of the trends observed in the experiments, including a weak compression wave at the separation corner for geometries with aft wall angles of 90 and 30 deg, an expansion wave at the separation corner for cavities with an aft-wall angle of 16 deg, essentially constant pressure along the lower cavity surface, and rapid compression along the aft wall due to shear-layer reattachment. Because unsteady results were expected for at least the rectangular geometries studied, the Reynolds-averaged simulation effort was not entirely successful. However, the quantitative agreement with the wall pressure measurements suggests that the time-averaged flowfield is well predicted. This comparison offers confidence that the simulations can be used to extract data that would be difficult to obtain by experiment alone. In particular, information

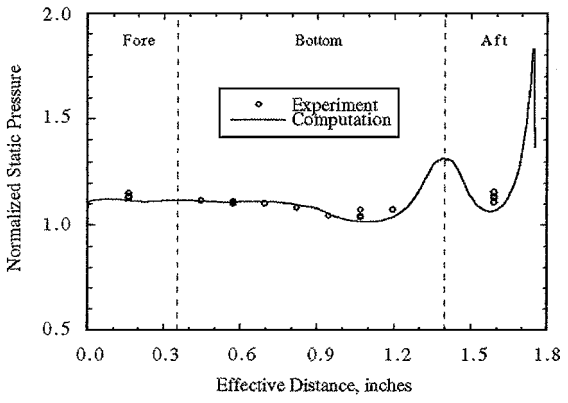

a) LD3-O1-90

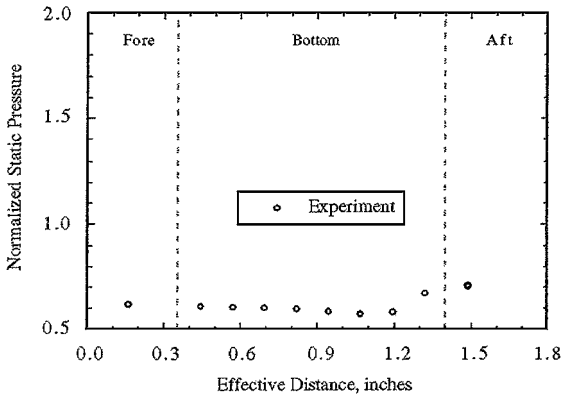

d) LD3-O2-90

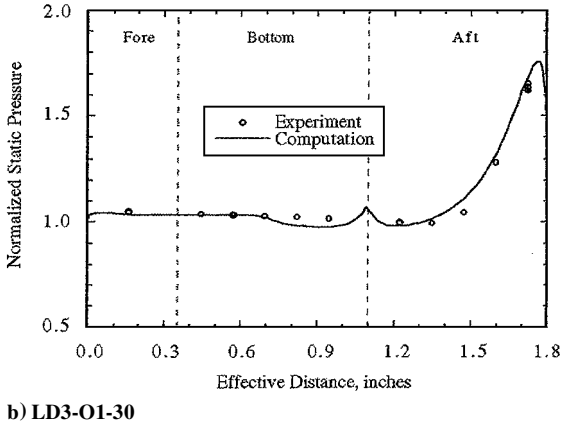

b) LD3-O1-30

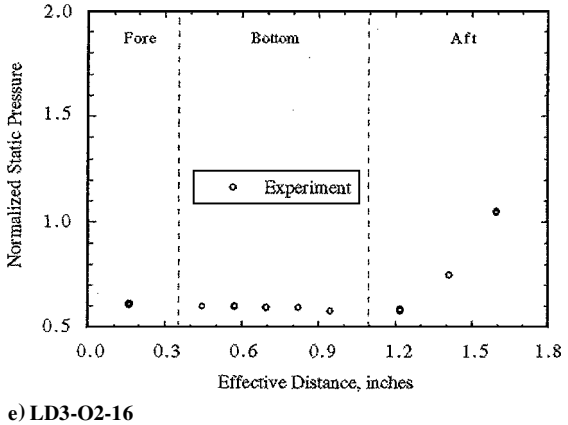

e) LD3-O2-16

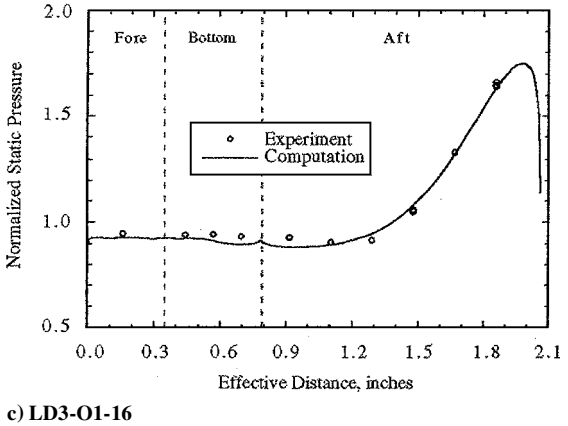

c) LD3-O1-16

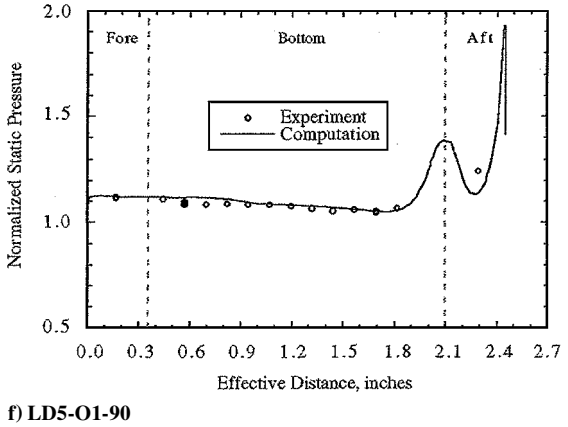

f) LD5-O1-90

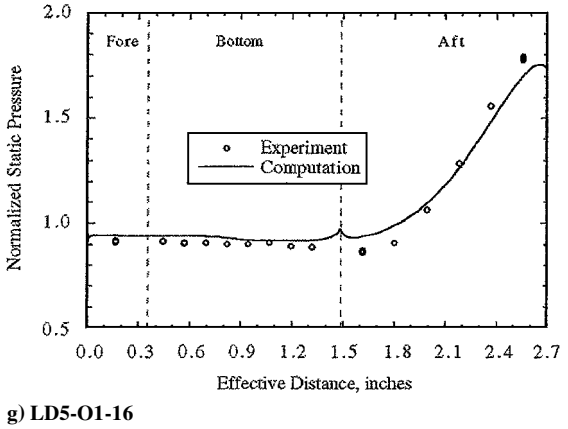

g) LD5-O1-16

Fig. 7 Experimental and computational wall static pressure distributions.

involving cavity residence time, and to a lesser extent drag, are difficult to deduce from a sparse set of surface measurements and flow images.

Cavity Residence Time

Cavity residence time is defined as the time scale associated with the decay rate of cavity fluid due to mass exchange with the mainstream. Winterfeld[3] studied flameholders in both isothermal and combusting flows. Results showed that residence time increased in the combusting cases whereas the exchange rate between the flameholder recirculation zone and the oxidizer stream decreased. Should this trend hold in the study of flameholders for scramjet applications, the residence times deduced in this cold-flow investigation would be less than those encountered during combustion (whereas the mass exchange rates would be overestimated). Nonetheless, the residence time deduced from a cold-flow CFD simulation can be used as input for simpler models to analyze kinetic issues within the cavity. In this case, the highly viscous cavity flow closely approximates the conditions required to use a perfectly stirred reactor concept.[6,37] Such a model can rapidly assess whether the cavity is of sufficient size to sustain combustion for a given fuel over some pressure and/or equivalence ratio range. In a cold-flow environment, the conservation equation governing a chemical species can be written as

$$\frac{\mathrm{d}m}{\mathrm{d}t} = -\frac{m}{\tau} \tag{1}$$

(where τ is residence time). Integration of Eq. (1) yields an exponential decay for the cavity mass:

$$m \sim \exp[-t/\tau] \tag{2}$$

Therefore, if the mass (or mass flow rate) is known as a function of time, then the residence time can be deduced. In this work, the cavity residence times were extracted from the CFD data in the following manner. Starting from a steady-state solution (or a solution where the oscillations are self-sustaining), the flow initially present in the cavity is tagged. The simulation is then executed in a time-accurate mode, and the tagged cavity fluid is monitored as it exits the domain. The time history of the cavity fluid mass is least-squares fit using Eq. (2) to find the residence time.

The residence times deduced from the CFD data are summarized in Table 2. The results show a consistent decrease in residence time as the aft ramp angle is reduced. The primary reason for this behavior lies in the structure of the recirculating flow within the cavity. The mass entrainment into the cavity is roughly proportional to the mainstream velocity.[6] Thus, cavity geometries that exhibit one large primary recirculation zone (i.e., geometries with small aft ramp angles) will exchange mass more readily than cavity geometries with a large embedded secondary vortex. The velocity on either side of the interface between the cavity vortices is much smaller than the mainstream velocity. Thus, the exchange rate between the two vortices is less than the exchange rate between the cavity and the main stream. Figure 8 shows the mass distribution within the LD3-01-90 cavity after approximately 3 ms have elapsed. The mass exchange between the vortices limits the net mass exchange rate with the crossflow. This phenomenon may be used to enhance the residence time while maintaining relatively small cavities. However, a scheme that takes advantage of this feature must also overcome the problem of transporting the appropriate combustible mixture into these structures. Previous simulations in subsonic combustors have shown that the sizes of the two vortices alternate in time. Thus, a time-dependent simulation is required to assess the influence of unsteadiness on the cavity flow.

Table 2 Calculated performance

Name	τ, ms	Pressure-drag coefficient	Viscous drag coefficient
LD3-O1-90	1.24	0.0166	$-3.7e{-}04$
LD3-O1-30	0.95	0.0272	$-6.2e{-}04$
LD3-O1-16	0.77	0.0435	$-4.4e{-}04$
LD5-O1-90	1.04	0.0277	$-8.1e{-}04$
LD5-O1-16	0.89	0.0490	$-4.7e{-}04$

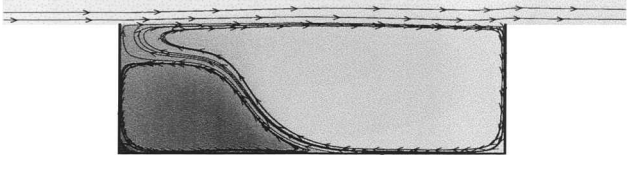

Fig. 8 LD3-O1-90 fuel distribution.

Increasing the cavity length did not significantly alter the residence time because the residence time is primarily dependent on the cavity depth. Lengthening the cavity increases its volume (increases τ), but the mass exchange rate is also increased (decreases τ). The secondary vortex in cavity LD3-O1- 90, rather than the dimensions of the cavity itself, causes the larger difference in residence time between the rectangular cavities.

Cavity Drag

Drag coefficients (drag force normalized by the freestream dynamic pressure and cavity fore wall area) for each cavity configuration appear in Table 2. As expected, the wave drag is the dominant component. The friction forces actually produce thrust due to the flow recirculation within the cavity. As the aft wall angle is reduced, the drag increases due to higher pressures acting over a larger fraction of the aft wall area. This results from the flow expansion into the cavity. Increasing L/D (for fixed depth) increases the drag slightly because the shear layer expands deeper into the cavity and exposes more of the aft wall to high pressures. A substantial increase in drag would appear if L/D were increased to the point of a closed cavity.

In general, decreasing the aft wall angle should promote both a more acoustically stable cavity flow (and subsequent stable burning) and improved entrainment because the shear layer impinges deeper into the cavity. However, smaller aft wall angles reduce cavity pressure. Furthermore, smaller aft wall angles increase the cavity drag and are expected to result in higher heat transfer rates to the cavity aft wall due to shear-layer reattachment. Based on these observations, a strong interdependence appears to exist between the desired cavity flameholder performance parameters and the cavity aft wall angle.

Conclusions

Flowfield properties of various cavity geometries were experimentally and computationally evaluated under Mach 3 flow conditions. Their flow characteristics were visualized using schlieren and shadowgraph techniques. The wall static pressure distributions were measured both along and off of the spanwise symmetry plane to assess the symmetry of the flowfield. Results indicate that the aft ramp angle plays a strong role in determining the character of the shear layer that spans the length of the cavity. Reductions in the aft ramp angle below 90 deg yield more stable, two-dimensional flowfields. The characteristics of the separation wave also change from compressive to expansive as the aft ramp angle is reduced. The cavity fore wall pressure steadily decreases with decreasing ramp angle. Calculated residence times and drag coefficients also highlight the importance of the aft ramp angle. Reductions in ramp angle result in higher drag coefficients and shorter residence times within the cavity. However, the flowfield becomes increasingly stable and two-dimensional.

For rectangular cavities, recompression is rapid with strong pressure gradients near the aft wall. These cases are also visibly unsteady as evidenced by the flow visualizations and the periodic waves that interact with the main separation and recompression shocks.

Changes in the offset ratio (OR) cause more drastic changes to the cavity flowfield. The separation wave is observed to be relatively strong and expansive in nature. The cavity fore wall experiences a much lower pressure in these cases than in any of the configurations where OR = 1. The shear layer dips much further into the cavity. The aft ramp angle has less influence on the overall cavity performance in these cases: no appreciable change in the pressure at the upstream face occurred as the ramp angle was decreased from 90 to 16 deg.

The recompression wave structure changed slightly in response to the decrease in aft ramp angle.

Experimental and computational pressure distributions agree closely for all configurations studied. Such agreement lends to confidence in the treatment of the turbulence modeling for obtaining time-averaged information, for example, wall pressure. Minor discrepancies were noted in the reattachment predictions in cavities with 90-deg ramp angles and OR = 1.

Future work on these configurations will involve measurements of entrainment rate, residence time, mixing behavior, and velocity field. Acoustic pressure levels will be characterized to substantiate the observed stabilizing effects of the aft ramp angle. Calculations will be extended to predictions of the unsteady flowfield using a large eddy simulation.

Acknowledgments

This work was funded by the Air Force Office of Scientific Research under the guidance of J. Tishkoff. The authors acknowledge the contributions of D. Schommer and W. Terry for their technical support. The support of the Research Air Facility is also appreciated.

References

[1]Mathur, T., Streby, G., Gruber, M., Jackson, K., Donbar, J., Donaldson, W., Jackson, T., Smith, C., and Billig, F., "Supersonic Combustion Experiments with a Cavity-Based Fuel Injector," AIAA Paper 99-2102, June 1999.

[2]Gruber, M., Jackson, K., Mathur, T., and Billig, F., "Experiments with a Cavity-Based Fuel Injector for Scramjet Applications," International Symposium on Air Breathing Engines, ISABE Paper IS-7154, Sept. 1999.

[3]Winterfeld, G., "On Processes of Turbulent Exchange Behind Flame Holders," *Tenth International Symposium on Combustion*, Combustion Inst., Pittsburgh, PA, 1965, pp. 1265–1275.

[4]Baurle, R. A., and Gruber, M. R., "A Study of Recessed Cavity Flowfields for Supersonic Combustion Applications," AIAA Paper 98-0938, Jan. 1998.

[5]Ben-Yakar, A., and Hanson, R., "Cavity Flameholders for Ignition and Flame Stabilization in Scramjets: Review and Experimental Study," AIAA Paper 98-3122, July 1998.

[6]Davis, D. L., "Numerical Analysis of Two and Three Dimensional Recessed Flame Holders for Scramjet Applications," Ph.D. Dissertation, Aeronautics and Astronautics Dept., Air Force Inst. of Technology, Wright–Patterson AFB, OH, Sept. 1996.

[7]Baysal, O., and Stallings, R. L., "Computational and Experimental Investigation of Cavity Flowfields," *AIAA Journal*, Vol. 26, No. 1, 1988, pp. 6, 7.

[8]Chokani, N., and Kim, I., "Suppression of Pressure Oscillations in an Open Cavity by Passive Pneumatic Control," AIAA Paper 91-1729, June 1991.

[9]Clark, R. L., Kaufmann, L. G., and Maciulaitis, A., "Aeroacoustic Measurements for Mach 0.6 to 3.0 Flows Past Rectangular Cavities," AIAA Paper 80-0036, Jan. 1980.

[10]Edwards, J. A., and Zhang, X., "Some Aspects of Supersonic Flow over a Cavity," AIAA Paper 86-2025, Aug. 1986.

[11]Franke, M. E., and Carr, D. L., "Effect of Geometry on Open Cavity Flow-Induced Pressure Oscillations," AIAA Paper 75-492, March 1975.

[12]Hankey, W. L., and Shang, J. S., "Analyses of Pressure Oscillations in an Open Cavity," *AIAA Journal*, Vol. 18, No. 8, 1980, pp. 892–898.

[13]Jeng, Y. N., and Payne, U. J., "Numerical Study of a Supersonic Open Cavity Flow and Pressure Oscillation Control," *Journal of Aircraft*, Vol. 32, No. 2, 1995, pp. 363–369.

[14]Kim, I., and Chokani, N., "Navier–Stokes Study of Supersonic Cavity Flowfield with Passive Control," *Journal of Aircraft*, Vol. 29, No. 2, 1992, pp. 217–223.

[15]Komerath, N. M., Ahuja, K. K., and Chambers, F. W., "Prediction and Measurement of Flows over Cavities—A Survey," AIAA Paper 87-0166, Jan. 1987.

[16]McGregor, O. W., and White, R. A., "Drag of Rectangular Cavities in Supersonic and Transonic Flow Including the Effects of Cavity Resonance," *AIAA Journal*, Vol. 4, No. 11, 1970, pp. 1959–1964.

[17]Morgenstern, A., and Chokani, N., "Hypersonic Flow Past Open Cavities," *AIAA Journal*, Vol. 32, No. 12, 1994, pp. 2387–2393.

[18]Perng, S. W., and Dolling, D. S., "Passive Control of Pressure Oscillations in Hypersonic Cavity Flow," AIAA Paper 96-0444, Jan. 1996.

[19]Rizzetta, D. P., "Numerical Simulation of Supersonic Flow over a Three-Dimensional Cavity," *AIAA Journal*, Vol. 26, No. 7, 1988, pp. 799–807.

[20]Rockwell, D., and Naudascher, E., "Review—Self-Sustaining Oscillations of Flow Past Cavities," *Journal of Fluids Engineering*, Vol. 100, No. 6, 1978, pp. 152–165.

[21]Sarno, R. L., and Franke, M. E., "Suppression of Flow-Induced Pressure Oscillations in Cavities," *Journal of Aircraft*, Vol. 31, No. 1, 1994, pp. 90–96.

[22]Vakili, A. D., Wolfe, R., Nagle, T., and Lambert, E., "Active Control of Cavity Aeroacoustics in High Speed Flows," AIAA Paper 95-0678, Jan. 1995.

[23]Zhang, X., and Edwards, J. A., "Computational Analysis of Unsteady Supersonic Cavity Flows Driven by Thick Shear Layers," *Aeronautical Journal*, Vol. 92, No. 919, 1988, pp. 365–374.

[24]Zhang, X., and Edwards, J. A., "An Investigation of Supersonic Oscillatory Cavity Flows Driven by Thick Shear Layers," *Aeronautical Journal*, Vol. 94, No. 940, 1990, pp. 355–364.

[25]Zhang, X., and Edwards, J. A., "Experimental Investigation of Supersonic Flow over Two Cavities in Tandem," *AIAA Journal*, Vol. 30, No. 5, 1992, pp. 1182–1190.

[26]Zhang, X., and Edwards, J. A., "A Computational Analysis of Supersonic Jet and Instability Wave Interaction," AIAA Paper 94-2194, June 1994.

[27]Zhang, X., "Compressible Cavity Flow Oscillation due to Shear Layer Instabilities and Pressure Feedback," *AIAA Journal*, Vol. 33, No. 8, 1995, pp. 1404–1411.

[28]Katta, V. R., and Roquemore, W. M., "Study on Trapped-Vortex Combustor: Effect of Injection on Flow Dynamics," *Journal of Propulsion and Power*, Vol. 14, No. 3, 1998, pp. 273–281.

[29]Hsu, K.-Y., Goss, L. P., and Roquemore, W. M., "Characteristics of a Trapped-Vortex Combustor," *Journal of Propulsion and Power*, Vol. 14, No. 1, 1998, pp. 57–65.

[30]Niioka, T., Terada, K., Kobayashi, H., and Hasegawa, S., "Flame Stabilization Characteristics of Strut Divided into Two Parts in Supersonic Airflow," *Journal of Propulsion and Power*, Vol. 11, No. 1, 1995, pp. 112–116.

[31]Yu, K., Wilson, K. J., Smith, R. A., and Schadow, K. C., "Experimental Investigation on Dual-Purpose Cavity in Supersonic Reacting Flows," AIAA Paper 98-0723, Jan. 1998.

[32]Vinogradov, V., Grachev, V., Petrov, M., and Sheechman, J., "Experimental Investigation of Two-Dimensional Dual Mode Scramjet with Hydrogen Fuel at Mach 4–6," AIAA Paper 90-5269, Oct. 1990.

[33]Vinogradov, V., Kobigsky, S., and Petrov, M., "Experimental Investigation of Liquid Carbonhydrogen Fuel Combustion in Channel at Supersonic Velocities," AIAA Paper 92-3429, July 1992.

[34]Vinogradov, V. A., Kobigsky, S. A., and Petrov, M. D., "Experimental Investigation of Kerosene Fuel Combustion in Supersonic Flow," *Journal of Propulsion and Power*, Vol. 11, No. 1, 1995, pp. 130–134.

[35]Romankov, O. N., and Starostin, F. I., "Design and Investigation of the Stand and Flying Scramjet Models Conceptions and Results of Experiments," AIAA Paper 93-2447, June 1993.

[36]McClinton, C., Roudakov, A., Semenov, V., and Kopehenov, V., "Comparative Flow Path Analysis and Design Assessment of an Axisymmetric Hydrogen Fueled Scramjet Flight Test Engine at a Mach Number of 6.5," AIAA Paper 96-4571, Nov. 1996.

[37]Nestler, D. E., Saydah, A. R., and Auxer, W. L., "Heat Transfer to Steps and Cavities in Hypersonic Turbulent Flow," AIAA Paper 68-673, June 1968.

[38]Baurle, R. A., Mathur, T., Gruber, M. R., and Jackson, K. R., "A Numerical and Experimental Investigation of a Scramjet Combustor for Hypersonic Missile Applications," AIAA Paper 98-3121, July 1998.

[39]Jackson, K., Gruber, M., Mathur, T., Streby, G., Smith, C., and Billig, F., "Calibration of a Newly Developed Direct-Connect High-Enthalpy Supersonic Combustion Research Facility," AIAA Paper 98-1510, April 1998.

[40]Gruber, M. R., and Nejad, A. S., "New Supersonic Combustion Research Facility," *Journal of Propulsion and Power*, Vol. 11, No. 5, 1995, pp. 1080–1083.

[41]White, J., "A Pseudo-Temporal Multigrid Relaxation Scheme for Solving the Parabolized Navier–Stokes Equations," AIAA Paper 99-3360, June 1999.

[42]Edwards, J. R., "A Low-Diffusion Flux-Splitting Scheme for Navier–Stokes Calculations," *Computers & Fluids*, Vol. 26, No. 6, 1997, pp. 635–659.

[43]Wilcox, D. C., *Turbulence Modeling for CFD*, DCW Industries, Inc., La Cadnada, CA, 1998.

[44]Wilcox, D. C., "Wall Matching, a Rational Alternative to Wall Functions," AIAA Paper 89-0611, Jan. 1989.

[45]Zeman, O., "Dilatational Dissipation: The Concept and Application in Modeling Compressible Mixing Layers," *Physics of Fluids*, Vol. 2, No. 2, 1990, pp. 178–188.

[46]Sarkar, S., Erlebacher, G., Hussaini, M. Y., and Kreiss, H. O., "The Analysis and Modeling of Dilatational Terms in Compressible Turbulence," NASA, Inst. for Computer Applications in Science and Engineering Rept. 89-79, 1989.